Biosensors and Bioelectronics 131 (2019) 299–306

Contents lists available at ScienceDirect

Biosensors and Bioelectronics

journal homepage: www.elsevier.com/locate/bios

A sandwich-type photoelectrochemical immunosensor for NT-pro BNP detection based on F-Bi_2WO_6/Ag_2S and GO/PDA for signal amplification

Yanrong Qian[a], Jinhui Feng[a], Dawei Fan[a], Yong Zhang[a], Xuan Kuang[a], Huan Wang[a,*], Qin Wei[a,*], Huangxian Ju[a,b]

[a] Key Laboratory of Interfacial Reaction & Sensing Analysis in Universities of Shandong, School of Chemistry and Chemical Engineering, University of Jinan, Jinan 250022, China

[b] State Key Laboratory of Analytical Chemistry for Life Science, Department of Chemistry, Nanjing University, Nanjing 210023, China

ARTICLE INFO

Keywords:
Flower-like Bi_2WO_6
Amino-terminal pro-B-type natriuretic peptide
Photoelectrochemical immunosensor
Polydopamine

ABSTRACT

A sandwich-type photoelectrochemical (PEC) immunosensing platform was designed for detection of amino-terminal pro-B-type natriuretic peptide (NT-pro BNP). Thereinto, flower-like Bi_2WO_6/Ag_2S nanoparticles (F-Bi_2WO_6/Ag_2S) were employed as photoelectrochemical matrix, and graphene oxide and polydopamine composite (GO/PDA) were prepared as signal labels. In this proposal, Ag_2S was in-situ growth on the surface of F-Bi_2WO_6 modified with thioglycolic acid (TGA). Specially, a cascade-like band-edge level between F-Bi_2WO_6 and Ag_2S effectively improved the photocurrent conversion efficiency and enhanced the photocurrent response. Then, the conjugated GO/PDA aimed to further amplify signal because PDA as electron donor could sweep the holes and inhibit the recombination of photogenerated electron-hole pairs, while GO owned brilliant conductivity speeding up the electrons transfer. The photocurrent increased with the amount of GO/PDA conjugates which had positive correlation with the NT-pro BNP. Under optimal experimental conditions, the proposed sandwich-type PEC immunosensor presented a desirable linear relationship ranged from 0.1 pg/mL to 100 ng/mL for NT-pro BNP with the detection limit of 0.03 pg/mL (S/N = 3). The prepared PEC immunosensor exhibited high stability and selectivity, which offered an innovative idea for the detection of other biomolecules.

1. Introduction

Heart failure has been known as a disease in which the ability of heart is insufficient to meet the body's blood circulation need (Liquori et al., 2014; Tian et al., 2014). At present, heart failure has been concerned all over the world in the grim situation where more than 20 million people suffer from the disease (Richards and Troughton, 2014). According to reports, the amino-terminal pro-B-type natriuretic peptide (NT-pro BNP) is one of the most important biochemical markers for the diagnostics and prognostics of heart failure (Weber et al., 2005). In addition, the level of NT-pro BNP is relevant to the identification of lower-degree heart failure (de Ávila et al., 2013; Hunt et al., 1995). The age-specific serum NT-pro BNP cut-points which had been proven to identify HF patients were as follows: (1) > 1800 pg/mL in patients > 75 years old; (2) > 900 pg/mL in patients aged 50–75 years old; and (3) > 450 pg/mL in patients < 50 years old (Liu et al., 2018). Therefore, looking for an effective method to detect NT-pro BNP is important for the early diagnosis and prevention of heart failure.

Photoelectrochemical (PEC) bioanalysis, a newly emerging and rapidly developing detection method, has attracted substantial research scrutiny due to the advantages of low cost, simple instrumentation, and easy to micromation (P.P. Liu et al., 2017; Xue et al., 2017; Zhang et al., 2017; Zhao et al., 2015). It is worth noting that PEC bioanalysis possesses good sensitivity because of the separation of excitation source and the detection signal based on the energy conversion from light power to electric power (Zhou et al., 2017). PEC immunoassay plays a key role in the field of bioassay relying on the inherent sensitivity of the PEC bioanalysis and the specific bio-affinity properties of the immunomolecules (Zhao et al., 2017). What is more, the sensitivity is also affected by the photocurrent which is generated by photoactive substance. Thence, photoactive material is an important part of PEC immunosensors.

Bi_2WO_6, a kind of multicomponent semiconductor oxide, is one of the simplest Aurivillius oxides with possessing layered structure (Rangel, 2002; Zhang et al., 2007). Recently, Bi_2WO_6 has been applied in various fields due to its excellent photoactivity. For example, Cheng et al. (2012) took advantage of Bi_2WO_6 hollow microspheres for photocatalytic reduction of CO_2 under the efficient visible light. Zhang

* Corresponding authors.
E-mail addresses: chm_wanghuan@ujn.edu.cn (H. Wang), chm_weiq@ujn.edu.cn (Q. Wei).

https://doi.org/10.1016/j.bios.2019.02.029
Received 15 November 2018; Received in revised form 27 January 2019; Accepted 11 February 2019
Available online 19 February 2019
0956-5663/

et al. (2013) reported that Bi_2WO_6 was used as a highly selective visible-light photocatalyst toward oxidation of glycerol to dihydroxyacetone in water. Morphology is an important factor affecting the performance of the materials and thus has an effect on the property of the sensors (Shi et al., 2013) and the 3D structures are critical to realize a large accessible surface area (Shi et al., 2017). The flower-like Bi_2WO_6 (F-Bi_2WO_6) has attracted much attention because of large specific surface area and plenty of mesopores with ordered open pore frameworks, which can effectively harvest irradiation light (Li et al., 2012; Liang et al., 2015). However, the pure Bi_2WO_6 has the poor utilization of visible light because the light absorption is shorter than 450 nm (Z. Zhang et al., 2010). In order to improve the utilization of visible light, combining F-Bi_2WO_6 with narrow bandgap semiconductors is an efficacious way. Ag_2S nanoparticles, a narrow bandgap semiconductor (about 1 eV), attract broad attentions because of low-toxicity, good chemical stability and excellent optical limiting properties (Neves et al., 2009; Wang et al., 2010). Over here, Ag_2S was in situ growth on the surface of F-Bi_2WO_6, which were modified with thioglycolic acid (TGA) for improving the photoelectric response. Most importantly, a cascade-like band-edge level between Ag_2S and Bi_2WO_6 is beneficial to promote the electrons transfer and prohibit the recombination of photogenerated electron-hole pairs, leading to a strong and stable photoelectric response.

In addition, labels conjugated with secondary antibodies (Ab_2) play a principal role for a sandwich-type PEC immunosensor. Reducing the recombination of photogenerated electron-hole pairs is one of the most effective means for highly sensitive detection (X. Wang et al., 2017). Accelerating the electrons transfer is advantageous for suppressing the recombination of photogenerated electron-hole pairs. Polydopamine (PDA), a mimic of the specialized adhesive foot protein, is obtained through biocompatible self-polymerization product of dopamine (DA) (Guo et al., 2012; Lin et al., 2014; Ma et al., 2017). Simultaneously, there are many functional groups on the PDA, such as abundant amino, hydroxyl groups and so on (Xing et al., 2018). PDA could directly conjugate molecules via Michael addition or Schiff base reaction without other complicated process (LaVoie et al., 2005; Longo et al., 2015; Mauchauffé et al., 2016). Therefore, PDA is easy to connect with the Ab_2 without any treatment. Other than that, much conjugated polymer chains can facilitate the photoinduced charges separation, which enhances the photocurrent conversion efficiency (J. Li et al., 2017). What is more, the PDA was used not only as electron donor to get rid of the holes inhabiting the recombination of photoinduced charges but also as a cross-linker reagent for the immobilization of Ab_2 (R. Wang et al., 2017). Graphene oxide (GO), a carbon-based nanomaterial, is known for the large specific surface area, outstanding electronic conductivity and high carrier mobility (Zhang et al., 2014; Zhu et al., 2016). Here, GO was used as one of the markers to load PDA for further signal amplification in this proposal. In short, we exploited the GO/PDA as labeled conjugates to amplify signal.

We proposed a sandwich-type PEC immunosensor to detect NT-pro BNP utilizing F-Bi_2WO_6/Ag_2S NPs as matrix and GO/PDA as signal labels though layer-by-layer strategy. The Ag_2S was in-situ growth on the surface of F-Bi_2WO_6 by strong coordination interactions between sulfhydryl groups of TGA and Bi atoms of F-Bi_2WO_6. In addition, GO/PDA combining via classical coupling reaction between carboxyl and amino groups was used as a signal amplifier for the first time.

2. Experimental section

2.1. Materials and reagents

Thioglycolic acid (TGA) and sodium tungstate (Na_2WO_4) were purchased from Kermel Chemical Reagent Co. Ltd. (Tianjin, China). NT-pro BNP, NT-pro BNP primary antibody (Ab_1) and NT-pro BNP secondary antibody (Ab_2) were purchased from Shanghai Linc-Bio Science Co., Ltd. (Shanghai, China). The other details are provided in Supplementary Material (SM).

2.2. Apparatus

All PEC experiments were carried out on a CHI760E electrochemical workstation (Shanghai Chenhua Instruments Co., Ltd, China). A three-electrode system including a platinum wire electrode as counter electrode, a saturated calomel electrode as reference electrode and modified indium tin oxide electrode (ITO) ($2.5 \times 0.8\ cm^2$) as the working electrode was used for PEC measurements. The other details can be found in SM.

2.3. Preparation of the F-Bi_2WO_6

The synthesis of the F-Bi_2WO_6 was according to the reported literature with slightly modified (L. Zhang et al., 2010). The specific synthesis is provided in SM.

2.4. Preparation of GO/PDA-Ab_2

GO was prepared by a modified Hummers' method from graphite powder (Yin et al., 2011). On the basis of the previous report, PDA was synthesized through oxidative polymerization of dopamine (DA) (Y. Liu et al., 2017). The other details can be found in SM. The preparation of GO/PDA-Ab_2 was ascribed to the literature with a few changes (R. Wang et al., 2017). Firstly, 80 mg GO was dispersed in 80 mL of ultrapure water under ultrasonic processing for 8 h. Hereafter, the above solution and 8 mL of PDA solution were mixed with magnetically stirring. Next, the resulting mixture shook for 24 h. Then, the above system filtered and washed three times. Finally, the GO/PDA was obtained after freeze drying. Then, 2 mg GO/PDA was dispersed into 1 mL of 5 μg/mL Ab_2 solution. The resulting system shook at 4 °C for 12 h and then the unbound Ab_2 was removed by continuously centrifugation. Finally, the desired GO/PDA-Ab_2 was acquired and redistributed in 1 mL of 0.1 mol/L phosphate buffer solution (PBS, pH 7.4).

2.5. Fabrication of the PEC immunosensor

As illustrated in Scheme 1, a sandwich-type PEC immunosensor was established. Prior to use, the bare ITO electrodes were ultrasonically cleaned orderly in acetone, ethanol and ultrapure water for about 30 min. After that, the ITO slices dried with the nitrogen stream. Specifically, 10 μL of 11 mg/mL F-Bi_2WO_6 homogeneous suspension was dropped onto the treated ITO electrode. After being dried, the ITO/F-Bi_2WO_6 electrode was calcined at 550 °C for 2 h in air atmosphere and naturally cooled to room temperature. Next, the Ag_2S was deposited on the above electrode in accordance with successive ionic layer adsorption and reaction strategy. First of all, 4 μL of 0.1 mol/L TGA was dropped on the calcined ITO/F-Bi_2WO_6 electrode surface and naturally dried. After washing with ultrapure water, 4 μL of 0.14 mol/L $AgNO_3$ solution was dropped onto the surface of resulting electrode and dried under darkness. Then, 4 μL of 0.2 mol/L Na_2S solution was dropped onto the above electrode to make Ag_2S full growth at the room temperature, then washed the ITO/F-Bi_2WO_6/Ag_2S electrode to remove excess Ag_2S thoroughly. The desired ITO/F-Bi_2WO_6/Ag_2S electrode was obtained.

4 μL of 3 mmol/L TGA was dropped onto the ITO/F-Bi_2WO_6/Ag_2S electrode. After dried and washed with ultrapure water, the resulting electrode was modified with 1-ethyl-3-(3-dimethylaminopropyl) carbodiimide hydrochloride and N-hydroxysuccinimide (EDC/NHS) containing 1×10^{-2} mol/L EDC and 2×10^{-3} mol/L NHS. After washing off the excess EDC/NHS, 6 μL of 10 μg/mL Ab_1 was immobilized on the above electrode at 4 °C for 1 h. To block the non-specific active sites, 3 μL of 1 wt% bovine serum albumin (BSA) was dropped onto the

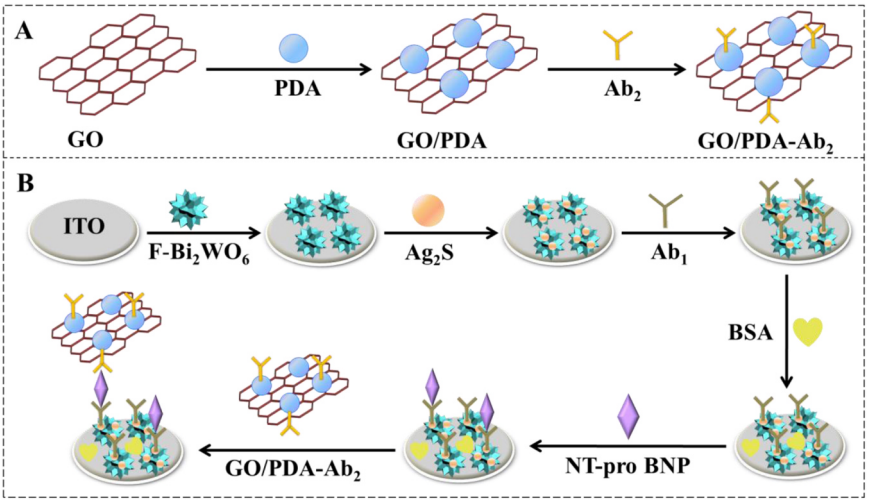

Scheme 1. (A) Synthesis process of GO/PDA-Ab_2; (B) Fabrication process of the sandwich-type PEC immunosensor for NT-Pro BNP detection.

electrode. After that step, the different concentrations of NT-pro BNP were dropped onto above modified electrodes and then incubated at 4 °C for 1 h. After the immunoreaction between Ab_1 and NT-pro BNP, the above electrodes were labeled with 6 μL of 2 mg/mL GO/PDA-Ab_2 solution incubating at 4 °C for 1 h. The electrodes were cleaned by 0.1 mol/L PBS (pH 7.4) after each step. Finally, the sandwich-type PEC immunosensor was well-fabricated and stored in a 4 °C refrigerator for the further photocurrent measurement.

2.6. PEC detection

The PEC measurements were implemented making use of a PEC workstation with a conventional three-electrode system in 0.1 mol/L PBS (pH 7.4) containing a certain amount of ascorbic acid (AA). The photocurrent signal was tested by the current-time curve. The 100 W LED lamp, a white light, was used as the irradiation source (Using the white light as an excitation source could improve the utilization rate of light source and the white light was inexpensive compared with the single wavelength light). During the PEC test, the lamp was switched on and off every 10 s resulting in the signal on and off. The applied voltage was 0 V.

3. Results and discussion

3.1. Characterization of F-Bi_2WO_6/Ag_2S and GO/PDA

The prepared materials were characterized by scanning electron microscope (SEM). As shown in Fig. 1A, the prepared Bi_2WO_6 was flower-like structure with relatively uniform size. Fig. 1B was a further enlarged SEM image of F-Bi_2WO_6. It could be seen that the F-Bi_2WO_6 with a mean diameter about 1 μm. As shown in Fig. 1C, the Ag_2S was successfully deposited on the surface of F-Bi_2WO_6. The TEM images of F-Bi_2WO_6 and F-Bi_2WO_6/Ag_2S (Fig. S4A and C) also clearly displayed the flower-like shape of F-Bi_2WO_6, which were well consistent with the SEM results. Meanwhile, the high-resolution TEM (HRTEM) images (Fig S4B and D) also identified distinct crystal lattice fringes of F-Bi_2WO_6 and Ag_2S, which further confirmed the existence of Ag_2S on the F-Bi_2WO_6. Energy dispersive spectrometry (EDS) was used to show the element composition of substance. W, O and Bi were existed in F-Bi_2WO_6 as shown in Fig. S1A and Fig. S1B indicated that the F-Bi_2WO_6/Ag_2S included Bi, W, O, Ag and S elements, which illustrated the F-Bi_2WO_6 and F-Bi_2WO_6/Ag_2S were prepared successfully. Fig. 1D displayed that PDA were nanospheres with an average diameter of 300 nm. Fig. 1E showed the morphology of GO was flake-like structure. As illustrated in Fig. 1F, it revealed that PDA was evenly distributed and grown on GO, which indicated the successful synthesis of GO/PDA.

The X-ray diffraction (XRD) pattern of F-Bi_2WO_6 and F-Bi_2WO_6/Ag_2S was shown in Fig. 1G. The diffraction peaks of F-Bi_2WO_6 (curve a) appearing at 28.30, 32.91, 47.14, 55.99, 76.08, 78.53 could be corresponded to the (131), (002), (202), (133), (2102), (204) planes of Bi_2WO_6 (JCPDS 39-0256), which indicated the F-Bi_2WO_6 was successfully synthesized. Moreover, the pattern did not contain the diffraction peaks of any other phases or impurities, which illustrated the high purity of as-prepared F-Bi_2WO_6. The diffraction peaks (curve b) appeared at 26.32, 28.97, 31.46, 34.37, 36.81 and 37.70 corresponding to (012), (111), (121), (112), (103) and (031), which could be indexed to Ag_2S (JCPDS 14-0072). It revealed that Ag_2S was loaded on the F-Bi_2WO_6. For all, the diffraction interference signal is not relatively large because the Ag_2S in-situ growth on the surface of F-Bi_2WO_6, the cover of Ag_2S made the exposure of crystal face reduce and the smaller size of the Ag_2S.

Fig. 1H displayed the UV–vis diffuse reflectance spectra of F-Bi_2WO_6, F-Bi_2WO_6-TGA and F-Bi_2WO_6/Ag_2S. The absorption edge of prepared F-Bi_2WO_6 (curve a) was 440 nm illustrating the poor utilization of light energy, which was ascribed to the wide band gap of F-Bi_2WO_6. The absorption of F-Bi_2WO_6-TGA (curve b) happened red shift compared with the absorption edge of F-Bi_2WO_6 due to strong coordination between sulfhydryl groups of TGA and Bi atoms of the as-prepared F-Bi_2WO_6 (Feng et al., 2018). However, the utilization of visible light was still poor at this moment. Thence, it was worthwhile to explore an effective and practical mean for taking advantage of light energy. Ag_2S as the narrow bandgap semiconductor of 1.0 eV was assembled on the surface of F-Bi_2WO_6, which made F-Bi_2WO_6/Ag_2S have a wide absorption of visible light (curve c).

The Fourier transform infrared spectroscopy (FTIR) spectrum of GO/PDA, PDA and GO was shown in Fig. 1I. The peaks at 3412 cm^{-1}, 1733 cm^{-1} and 1632 cm^{-1} were attributed respectively to stretching vibration of phenolic O-H, the C=O vibration and C-OH bending vibration, which demonstrated the existence of fruitful oxygen functional groups on GO. The adsorption peaks of pure PDA at 3429 cm^{-1} (stretching vibration of phenolic O-H and N-H), 1597 and 1492 cm^{-1} (the ring vibration of indole), 1375 cm^{-1} (phenolic C-O-H bending vibration), 1176 cm^{-1} (heterocyclic N-H in-plane deformation breathing) illustrated the presence of oxygen-containing functional groups in PDA. The reason why some peaks were available in GO (c) and PDA (b) but absent in GO/PDA (a) in FTIR spectrum was that PDA and GO were compounded by reactions between functional groups (Hu et al., 2014; Tu et al., 2012; Zheng et al., 2013). Because the composite of GO/PDA was owing to the valence bond instead of physical adsorption, the change of the peaks of functional groups in FTIR spectrum was

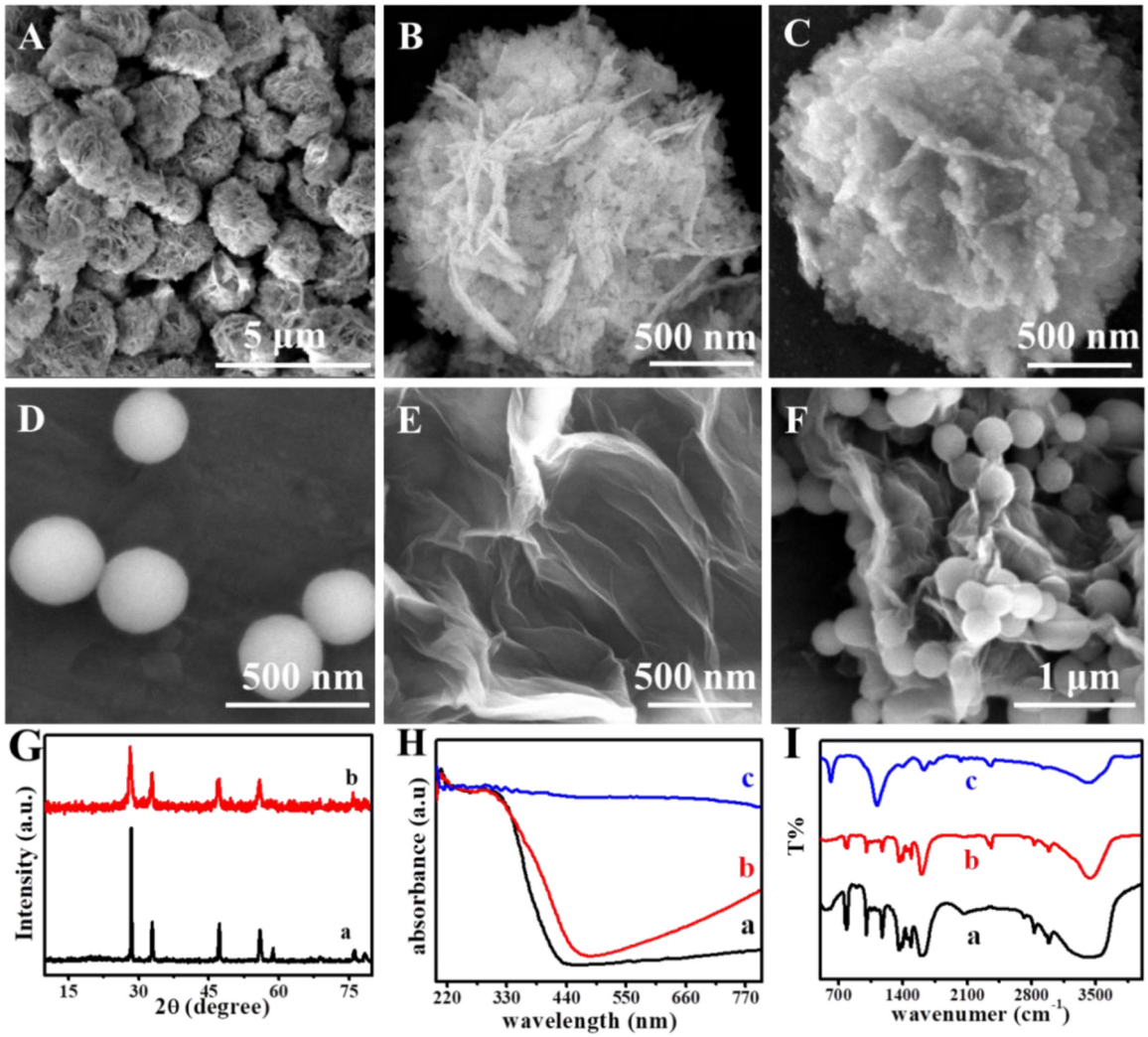

Fig. 1. SEM images of (A and B) F-Bi_2WO_6, (C) F-Bi_2WO_6/Ag_2S, (D) PDA, (E) GO and (F) GO/PDA, respectively; (G) XRD spectrum of (a) F-Bi_2WO_6, (b) F-Bi_2WO_6/Ag_2S; (H) UV–vis diffuse reflectance spectra of (a) F-Bi_2WO_6, (b) F-Bi_2WO_6-TGA and (c) F-Bi_2WO_6/Ag_2S; (I) FTIR spectrum of (a) GO/PDA, (b) PDA, (c) GO.

inevitable before and after compounding. Similarly, the GO/PDA of FTIR spectrum included both adsorption peaks of GO and PDA, which illustrated PDA had affinity to GO.

To investigate the chemical composition of F-Bi_2WO_6 and Ag_2S, the X-ray photoelectron spectroscopy (XPS) was carried out. As shown in Fig. S2A, the XPS survey spectra revealed that the F-Bi_2WO_6 was mainly composed of Bi, W, O elements and their homologous photoelectron peaks were Bi 4f, W 4f, and O 1s, respectively. Fig. S2B showed the high resolution Bi 4f XPS spectra of the sample, and the peaks were observed at 158.6 eV and 163.9 eV which could be assigned to Bi $4f_{7/2}$ and Bi $4f_{5/2}$, corresponding to Bi^{3+} in the crystal structure (Zhang et al., 2015). In Fig. S2C, peaks at 34.9 eV and 37.1 eV, corresponding to W $4f_{7/2}$ and W $4f_{5/2}$, could be attributed to a W^{6+} oxidation state of F-Bi_2WO_6 (Ryu et al., 2007); As shown in Fig. S2D, the peaks loaded at 529.8 eV and 531.0 eV were Bi–O bonds in$(Bi_2O_2)^{2+}$ slabs of Bi_2 WO_6 layered structure and hydroxyl groups on the surface, respectively (Tian et al., 2014). Typical survey XPS spectrum of Ag_2S (Fig. S3A) could be detected the Ag and S elements. As shown in Fig. S3B, two peaks with binding energies around 367.8 eV and 373.8 eV were corresponding to the Ag $3d_{5/2}$ and Ag $3d_{3/2}$ orbitals of Ag^+ in the structure. The peaks observed at 161.0 eV and 162.1 eV were assigned separately to the S $2p_{3/2}$ and S $2p_{1/2}$ owing to the S^{2-} in Ag_2S (Hu et al., 2016).

3.2. Characterization of the sandwich-type PEC immunosensor

In order to characterize interface properties of the electrodes, electrochemical impedance spectroscopy (EIS) is an effective way (Fan et al., 2016; Yang et al., 2017b). The impedance spectrum was measured in 5.0 mmol/L $[Fe(CN)_6]^{3-/4-}$ solution containing 0.10 mol/L KCl. Fig. 2A displayed impedance spectra of different electrodes undergoing different modification processes. Each impedance spectrum consists of two parts, one of which is the semicircular part representing electron-transfer process and the other is the linear part causing by the limited diffusion process. The inset of Fig. 2A is the equivalent circuit, including the solution resistance (R_s), the Warburg impedance (Z_ω), the double-layer capacitance (C_{dl}) and the electron transfer resistance (R_{et}) (Pang et al., 2018). The detailed value of them can be found in Table S1. Particularly, the R_{et} which can be measured by the semicircle diameter plays an important role in illustrating the interface properties of the electrodes. As shown in Fig. 2A, the bare ITO electrode (curve a) possessed the smallest value of R_{et}. Compared with the non-modified ITO electrode, the value of R_{et} always increased relatively after modifying F-Bi_2WO_6 (curve b) and Ag_2S (curve c) because of the weak conductivity of semiconductors. With the immobilization of Ab_1 (curve d) and BSA (curve e) onto the surface of electrodes in order, the R_{et}

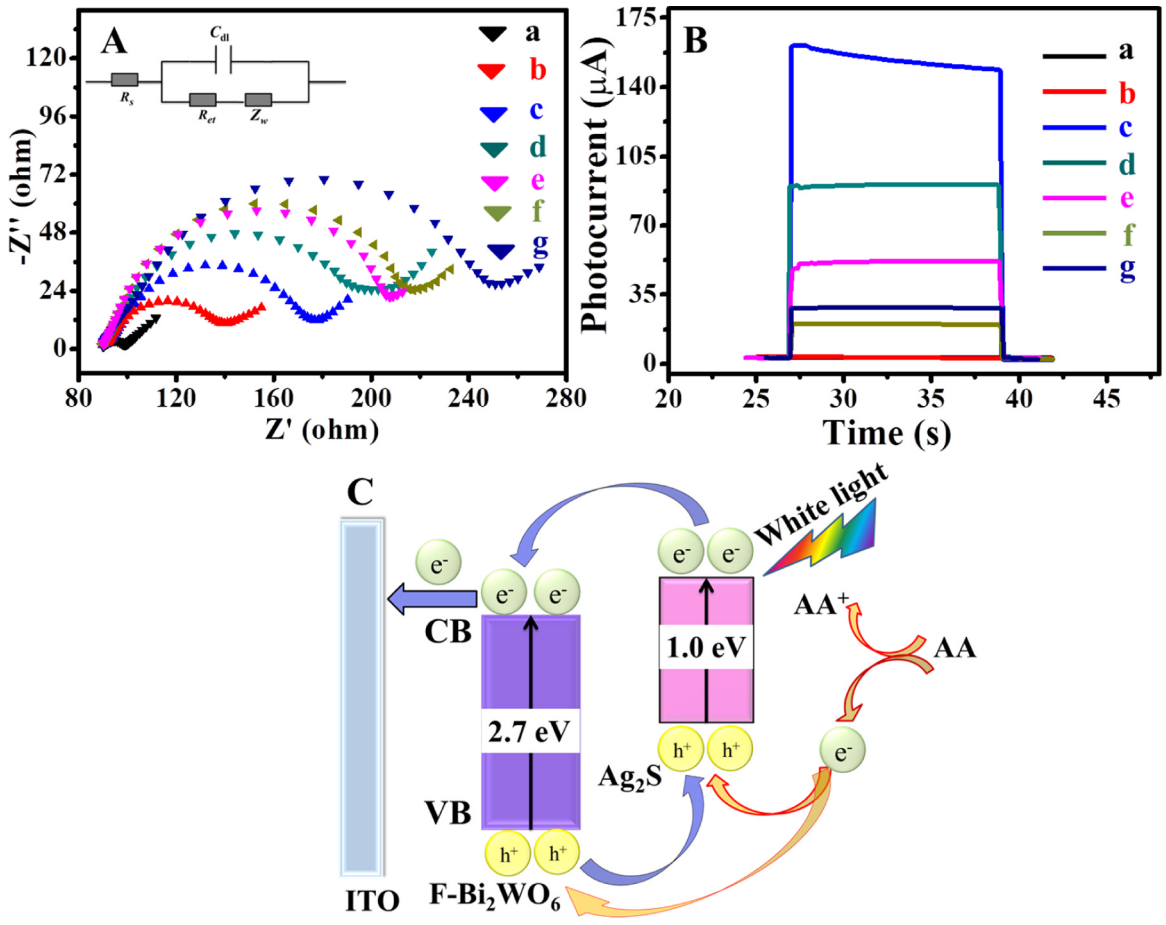

Fig. 2. (A) EIS Nyquist plots and (B) time-based photocurrent response curves of (a) ITO electrode, (b) after F-Bi_2WO_6 deposition, (c) after Ag_2S sensitization, (d) after Ab_1 incubation, (e) after BSA blocking, (f) after 1.0 ng/mL NT-Pro BNP incubation; (g) after GO/PDA-Ab_2 incubation. (C) The illustration of electron-transfer mechanism of PEC immunosensor based on F-Bi_2WO_6/Ag_2S in PBS solution containing AA. The inset in (A) is Randles equivalent circuit for EIS. The applied potential was 0 V.

increased gradually because the steric hindrances and insulating property of protein molecules. The value of R_{et} increased continuously after the NT-Pro BNP (curve f) and GO/PDA-Ab_2 (curve g) were successively incubated on the above electrode. These phenomena proved the successful construction of the sandwich-type PEC immunosensor.

Photocurrent measurement of layer-by-layer modified electrodes is another effective way to characterize the fabrication process of sandwich-type PEC immunosensor. As illustrated in Fig. 2B, the bare ITO electrode (curve a) exhibited no photocurrent signal. After modified the F-Bi_2WO_6 (curve b), the photocurrent value was almost close to zero because wide band gap energy of F-Bi_2WO_6. When the Ag_2S (curve c) was modified onto the ITO/F-Bi_2WO_6, the photocurrent was greatly increased owing to the deposited Ag_2S with a narrow band gap energy which increased the photocurrent conversion efficiency. As illustrated in Fig. 2C, the conduction band (CB) and valence band (VB) of Ag_2S were more negative than F-Bi_2WO_6. The electrons were excited from VB to CB of Ag_2S when irradiated by light, and then the excited electrons transferred from the CB of Ag_2S to the CB of F-Bi_2WO_6 under the irradiation of light, which inhabited the recombination of the photogenerated electron-hole pairs. The photocurrent decreased after modification of Ab_1 (curve d) and BSA (curve e) because of the insulation of protein molecules. When the NT-Pro BNP (curve f) was dropped on the electrode surface, the photocurrent continued to decrease. It could be explained that specific recognition of antigens and antibodies produced immunocomplex with the large steric hindrance. However, photocurrent increased after the GO/PDA-Ab_2 conjugates (curve g) were attached to the immunosensor. This might be owing to the electrical conductivity of GO and the effect of PDA. The change of photocurrent in each step indicated that the PEC immunosensor was successfully constructed.

3.3. Optimization of experimental conditions

For the sake of the superior performance of the sandwich-type PEC immunosensor, a series of conditions were optimized, such as the concentration of F-Bi_2WO_6, $AgNO_3$, AA, GO/PDA-Ab_2 and the pH value of PBS. When the experimental conditions were optimized, the method of control variates was utilized.

As shown in Fig. 3A, the concentration of F-Bi_2WO_6 had an influence on the photocurrent, which was examined from 6.0 to 12.0 mg/mL. When the concentration was less than 11.0 mg/mL, the photocurrent increased with the growing concentration of F-Bi_2WO_6. The photocurrent began to decrease when the concentration was greater than 11.0 mg/mL. Thus, 11.0 mg/mL was adopted as the optimal concentration of F-Bi_2WO_6 in this work (The other conditions were $AgNO_3$: 0.10 mol/L, AA: 0.10 mol/L, pH: 7.4 were in the ITO/F-Bi_2WO_6/Ag_2S electrodes). The content of Ag_2S which was affected by the concentration of $AgNO_3$ was an important factor affecting photocurrent. Fig. 3B displayed the change of photocurrent as the concentration of $AgNO_3$ ranged from 0.04 to 0.16 mol/L and the photocurrent reached a maximum when the concentration was 0.14 mol/L (The other conditions were F-Bi_2WO_6:11 mg/mL, AA: 0.1 mol/L, pH: 7.4 were in the ITO/F-Bi_2WO_6/Ag_2S electrodes). It might be explained that excellent photocurrent conversion efficiency of Ag_2S but similarly overmuch of Ag_2S

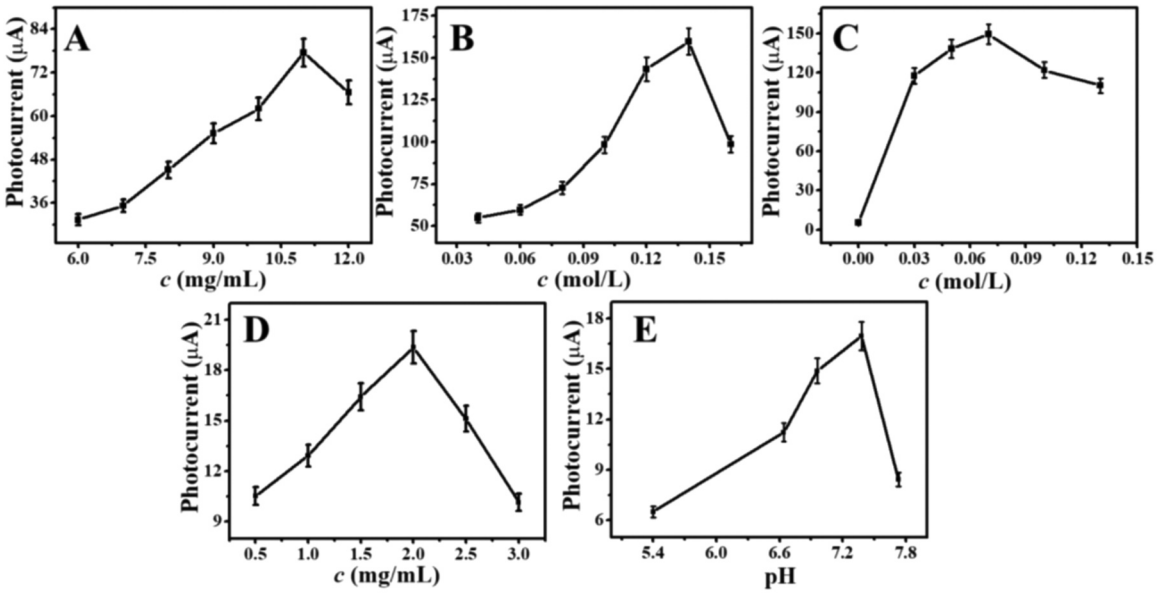

Fig. 3. Optimization of experimental conditions: (A) F-Bi_2WO_6 concentration, (B) $AgNO_3$ concentration, (C) AA concentration in the PBS on the photocurrent response of ITO/F-Bi_2WO_6/Ag_2S electrodes, (D) GO/PDA composite concentration on the photocurrent response of ITO/F-Bi_2WO_6/Ag_2S/Ab_1/BSA/NT-Pro BNP/GO/PDA-Ab_2 electrodes (E) the pH value of PBS. The applied potential was 0 V. For all studies, error bars = SD (n = 5).

blocked the electrons transfer. AA as electron donor can scavenge photogenerated holes to suppress the recombination of photogenerated electron-hole pairs. As shown in Fig. 3C, the photocurrent reached its maximum when the concentration of AA was 0.07 mol/L (The other conditions were F-Bi_2WO_6:11 mg/mL, $AgNO_3$: 0.14 mol/L, pH: 7.4 were in the ITO/F-Bi_2WO_6/Ag_2S electrodes).

Fig. 3D exhibited the effect of different concentrations of GO/PDA on photocurrent response and the concentration of 2.0 mg/mL was chosen as the optimum concentration (The other conditions were F-Bi_2WO_6: 11 mg/mL, $AgNO_3$: 0.14 mol/L, AA: 0.07 mol/L, pH: 7.4 were in ITO/F-Bi_2WO_6/Ag_2S/Ab_1/BSA/NT-Pro BNP/GO/PDA-Ab_2 electrodes). For the PEC immunosensor, the value of pH is a key factor in the process of measurement. The pH can affect the activity of biological proteins. The overly acidic or alkaline detection surroundings might damage the activity of the immobilized protein (X. Li et al., 2017). When the pH was 7.4, the photocurrent reached its maximum as illustrated in Fig. 3E (The other conditions were F-Bi_2WO_6: 11 mg/mL, $AgNO_3$: 0.14 mol/L, AA: 0.07 mol/L, GO/PDA: 2 mg/mL were in ITO/F-Bi_2WO_6/Ag_2S/Ab_1/BSA/NT-Pro BNP/GO/PDA-Ab_2 electrodes).

3.4. PEC detection for NT-Pro BNP

NT-Pro BNP detection was based on the sandwich-type immunoreactions. The photocurrent response of the immunosensor was directly connected with the concentration of NT-Pro BNP. Fig. 4A illustrated the variation of photocurrent at different concentrations of NT-Pro BNP. The photocurrent increased with the NT-Pro BNP concentration elevating because the more NT-Pro BNP was on the electrode and the more GO/PDA-Ab_2 conjugates were bounded onto the electrode. As a result, the photocurrent response and the concentration of NT-Pro BNP possessed an evident linear relationship when the concentration of NT-Pro BNP from 0.1 pg/mL to 100 ng/mL as shown in Fig. 4B. Moreover, the linear equation was $I = 21.19 + 2.27 \lg c$, and the correlation coefficient was 0.9954. The limit of detection for NT-Pro BNP concentration was calculated to be 0.03 pg/mL (S/N = 3). Compared with the previous reports (Table S2) and (Table S4), the fabricated PEC immunosensor was desirable with relatively wider linear range and a lower detection limit.

3.5. Selectivity, stability and reproducibility

Selectivity plays a crucial role in the evaluation of the PEC immunosensor (Ren et al., 2017a). To validate the selectivity of the proposed immunosensor, carcino-embryonic antigen (CEA), prostate-specific antigen (PSA) and insulin were used as potential interferences to study under the identical surroundings. The selectivity was tested by measuring the photocurrent of 1.0 ng/mL NT-Pro BNP containing 100 ng/mL interferences respectively. At the same time, the photocurrent was measured when 100 ng/mL CEA, PSA and insulin incubated on the blank electrodes respectively. As shown in Fig. 4C, the photocurrent change illustrated the excellent selectivity and specificity of the PEC immunosensor.

The stability of the developed immunosensor was evaluated by the photocurrent variation though consequent on/off irradiation cycles. Fig. 4D was obtained by the test of the immunosensor including 1.0 ng/mL NT-Pro BNP under several on/off irradiation cycles for a dozen times. There was no noticeable photocurrent change, which validated the stability of proposed immunosensor.

Reproducibility is another important parameter for evaluating the PEC immunosensor (Ren et al., 2017b; Yang et al., 2017a; Zhang et al., 2018). Aiming to assess the reproducibility, five PEC immunosensors containing 1.0 ng/mL NT-Pro BNP were prepared under the same conditions. The relative standard deviation (RSD) was 3.14% (21.39 μA, 21.61 μA, 21.83 μA, 20.83 μA, 22.69 μA), which explained the excellent reproducibility of the PEC immunosensor.

3.6. Real sample analysis

In order to further evaluate the feasibility and accuracy of the PEC immunosensors, the proposed PEC immunosensor was fabricated to detect the NT-Pro BNP in human serum sample by using the standard addition methods (Ren et al., 2017c). Firstly, the human serum sample was diluted with PBS before testing. The content of NT-Pro BNP in the

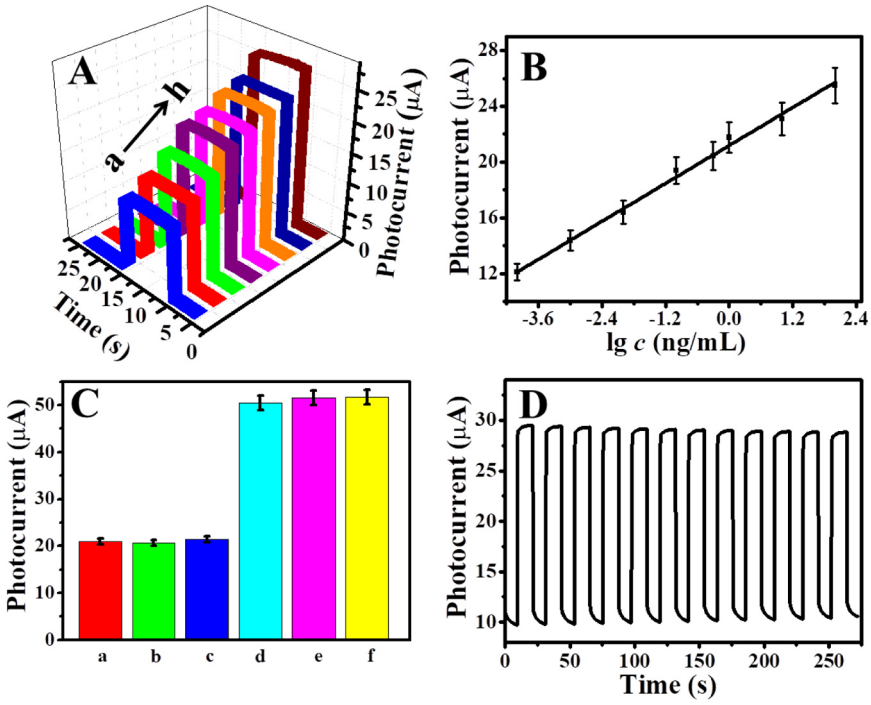

Fig. 4. (A) Photocurrent response curve and (B) the logarithmic calibration curve of the PEC immunosensor for detection of different concentrations of NT-Pro BNP: (a) 0.0001, (b) 0.001, (c) 0.01, (d) 0.1, (e) 0.5, (f)1, (g) 10, (h) 100 (Units: ng/mL). (C) Selectivity detection of the prepared PEC immunosensor for NT-Pro BNP. (a) 1.0 ng/mL NT-pro BNP + 100 ng/mL CEA; (b) 1.0 ng/mL NT-pro BNP + 100 ng/mL PSA; (c) 1.0 ng/mL NT-pro BNP + 100 ng/mL insulin; (d) 100 ng/mL CEA; (e) 100 ng/mL PSA; (f) 100 ng/mL insulin; (D) Stability evaluation of the PEC immunosensor under several on/off irradiation cycles, $c_{\text{NT-Pro BNP}}$ = 1.0 ng/mL. The applied potential was 0 V.

Table 1
NT-Pro BNP detection in human serum sample by prepared PEC immunosensor.

Initial NT-proBNP in the serum (ng/mL)	Added amounts (ng/mL)	Detection amounts (ng/mL)	RSD (%,n = 5)	Recovery (%)
0.23	0.10	0.34,0.33,0.33,0.32,0.34	2.5	102
	0.25	0.47,0.50,0.50,0.46,0.49	3.8	101
	0.50	0.70,0.74,0.76,0.71,0.72	3.3	99.2

human serum sample was obtained by five measurements using the proposed PEC immunosensor. Next, in order to assess the accuracy of the results, different concentrations of NT-Pro BNP were added into the above measured sample and tested by the PEC immunosensor again. Finally, the RSD and the recovery were calculated according to the test results. The results were shown in the Table 1. As a result, the recoveries were 102%, 101% and 99.2%, respectively, suggesting that this PEC immunosensor could meet the requirements of the human serum sample test. To further verify the accuracy of the analytical method, the biomarker of different human serum samples was measured by the proposed PEC immunosensor, and compared with the accepted analytical method (ELISA). The results were shown in Table S3. As a result, the relative deviation of the two methods was less than 5%, suggesting this PEC immunosensor was accurate.

4. Conclusion

In a word, a sandwich-type photoelectrochemical immunosensor was successfully fabricated for the detection of NT-Pro BNP based on the F-Bi_2WO_6/Ag_2S and GO/PDA. As a result of the three-dimensional flower structure, F-Bi_2WO_6 has the large specific surface to load the Ag_2S nanoparticles for obtaining the excellent photocurrent, creating an enabling environment for the proposed sensor. The GO/PDA as a signal amplification label made the photocurrent intensity increase owing to excellent electrical conductivity of GO and the effect of PDA. Based on the above advantages, the immunosensor achieved to NT-Pro BNP detection with a broad liner range of 0.1 pg/mL to 100 ng/mL with an ultralow detection limit of 0.03 pg/mL. Moreover, the resulting immunosensor for quantitative detection of NT-Pro BNP possesses excellent stability and satisfactory reproducibility. The proposed photoelectrochemical immunosensor provided a possibility for the detection of disease-related biomarkers.

CRediT authorship contribution statement

Yanrong Qian: Data curation, Investigation, Visualization, Writing - original draft. **Jinhui Feng:** Conceptualization, Formal analysis, Methodology. **Dawei Fan:** Supervision, Writing - review & editing. **Yong Zhang:** Supervision, Writing - review & editing. **Xuan Kuang:** Supervision, Writing - review & editing. **Huan Wang:** Conceptualization, Formal analysis, Methodology. **Qin Wei:** Project administration, Resources. **Huangxian Ju:** Project administration, Resources.

Acknowledgments

This study was supported by Natural Science Foundation of Shandong Province, China (No. ZR2017BB030), National Key Scientific Instrument and Equipment Development Projects of China (No. 21627809), National Natural Science Foundation of China (Nos. 21575050 and 21675063).

Declaration of interests

None.

Appendix A. Supporting information

Supplementary data associated with this article can be found in the online version at doi:10.1016/j.bios.2019.02.029.

References

Cheng, H., Huang, B., Liu, Y., Wang, Z., Qin, X., Zhang, X., Dai, Y., 2012. Chem. Commun. 48, 9729–9731.
de Ávila, B.E., Escamillagómez, V., Campuzano, S., Pedrero, M., Pingarrón, J.M., 2013. Anal. Chim. Acta 784, 18–24.
Fan, G.C., Zhu, H., Du, D., Zhang, J., Zhu, J.J., Lin, Y., 2016. Anal. Chem. 88, 3392–3399.
Feng, J., Li, Y., Gao, Z., Lv, H., Zhang, X., Fan, D., Wei, Q., 2018. Biosens. Bioelectron. 99, 14–20.
Guo, L., Liu, Q., Li, G., Shi, J., Liu, J., Wang, T., Jiang, G., 2012. Nanoscale 4, 5864–5867.
Hu, W., Guangli, H., Huanhuan, Z., Xiaoshuai, W., Jialin, L., Zhiliang, Z., Yan, Q., Zhisong, L., Yang, L., Chang Ming, L., 2014. Anal. Chem. 86, 4488–4493.
Hu, X., Li, Y., Tian, J., Yang, H., Cui, H., 2016. J. Ind. Eng. Chem. 45, 189–196.
Hunt, P.J., Yandle, T.G., Nicholls, M.G., Richards, A.M., Espiner, E.A., 1995. Biochem. Biophys. Res. Commun. 214, 1175–1183.
LaVoie, M.J., Ostaszewski, B.L., Weihofen, A., Schlossmacher, M.G., Selkoe, D.J., 2005. Nat. Med. 11, 1214–1221.
Li, J., Li, X., Zhao, Q., Tadé, M., Wang, S., Liu, S., 2017. Sens. Actuators B-Chem. 255, 133–139.
Li, X., Huang, R., Hu, Y., Chen, Y., Liu, W., Yuan, R., Li, Z., 2012. Inorg. Chem. 51, 6245–6250.
Li, X., Wang, Y., Shi, L., Ma, H., Zhang, Y., Du, B., Wu, D., Wei, Q., 2017. Biosens. Bioelectron. 96, 113–120.
Liang, Y., Lin, S., Li, L., Hu, J., Cui, W., 2015. Appl. Catal. B-Environ. 164, 192–203.
Lin, L.S., Cong, Z.X., Cao, J.B., Ke, K.M., Peng, Q.L., Gao, J., Yang, H.H., Liu, G., Chen, X., 2014. ACS Nano 8, 3876–3883.
Liquori, M.E., Christenson, R.H., Collinson, P.O., Defilippi, C.R., 2014. Clin. Biochem. 47, 327–337.
Liu, P.P., Liu, X., Huo, X.H., Tang, Y., Xu, J., Ju, H., 2017. ACS Appl. Mater. Interfaces 9, 27185–27192.
Liu, X.Y., Huang, Y.T., Lai, M.Y., Chen, J., Chu, T.W., Tsay, P.K., Shiao, C.C., 2018. Clin. Chim. Acta 480, 26–33.
Liu, Y., Zhao, Y., Zhu, Z., Xing, Z., Ma, H., Qin, W., 2017. Anal. Chim. Acta 963, 17–23.
Longo, J., Garnier, T., Mateescu, M., Ponzio, F., Schaaf, P., Jierry, L., Ball, V., 2015. Langmuir 31, 12447–12454.
Ma, H., Zhao, Y., Liu, Y., Zhang, Y., Wu, D., Li, H., Wei, Q., 2017. Anal. Chem. 89, 13049–13053.
Mauchauffé, R., Bonot, S., Moreno-Couranjou, M., Detrembleur, C., Boscher, N.D., Cécile, V.D.W., Duwez, A.S., Choquet, P., 2016. Adv. Mater. Interfaces 3, 1500520.
Neves, M.C., Nogueira, J.M.F., Trindade, T., Mendonça, M.H., Pereira, M.I., Monteiro, O.C., 2009. J. Photochem. Photobiol. A 204, 168–173.
Pang, X., Cui, C., Su, M., Wang, Y., Wei, Q., Tan, W., 2018. Nano Energy 46, 101–109.
Rangel, R., 2002. Surf. Rev. Lett. 9, 1779–1783.
Ren, X., Ma, H., Zhang, T., Zhang, Y., Yan, T., Du, B., Wei, Q., 2017a. ACS Appl. Mater. Interfaces 9, 37637–37644.
Ren, X., Yan, J., Wu, D., Wei, Q., Wan, Y., 2017b. ACS Sens. 2, 1267–1271.
Ren, X., Zhang, T., Wu, D., Yan, T., Pang, X., Du, B., Lou, W., Wei, Q., 2017c. Biosens. Bioelectron. 94, 694–700.
Richards, M., Troughton, R.W., 2014. Eur. J. Heart Fail. 6, 351–354.
Ryu, J.H., Bang, S.Y., Kim, W.S., Park, G.S., Kang, M.K., Yoon, J.W., Shim, K.B., Koshizaki, N., 2007. J. Alloy. Compd. 441, 146–151.
Shi, L., Chu, Z., Yu, L., Jin, W., Chen, X., 2013. Biosens. Bioelectron. 49, 184–191.
Shi, L., Yan, W., Ding, S., Chu, Z., Yu, Y., Jiang, D., Luo, J., Jin, W., 2017. Biosens. Bioelectron. 89, 871–879.
Tian, N., Zhang, Y., Huang, H., He, Y., Guo, Y., 2014. J. Phys. Chem. C 118, 15640–15648.
Tu, W., Wang, W., Lei, J., Deng, S., Ju, H., 2012. Chem. Commun. 48, 6535–6537.
Wang, D., Hao, C., Zheng, W., Peng, Q., Wang, T., Liao, Z., Yu, D., Li, Y., 2010. Adv. Mater. 20, 2628–2632.
Wang, R., Ma, H., Zhang, Y., Wang, Q., Yang, Z., Du, B., Wu, D., Wei, Q., 2017. Biosens. Bioelectron. 96, 345–350.
Wang, X., Rui, X., Xu, S., Wang, Y., Xiang, R., Du, B., Dan, W., Qin, W., 2017. Biosens. Bioelectron. 96, 239–245.
Weber, T., Auer, J., Eber, B., 2005. Curr. Pharm. Des. 11, 511–525.
Xing, B., Zhu, W., Zheng, X., Zhu, Y., Qin, W., Dan, W., 2018. Sens. Actuators B-Chem. 265.
Xue, L., Zhu, L., Zhou, Y., Yin, H., Ai, S., 2017. Anal. Chem. 89, 2369–2376.
Yang, L., Li, Y., Zhang, Y., Fan, D., Pang, X., Wei, Q., Du, B., 2017a. ACS Appl. Mater. Interfaces 9, 35260–35267.
Yang, L., Zhu, W., Ren, X., Khan, M.S., Zhang, Y., Du, B., Wei, Q., 2017b. Biosens. Bioelectron. 91, 842–848.
Yin, S., Zhang, Y., Kong, J., Zou, C., Li, C.M., Lu, X., Ma, J., Boey, F.Y., Chen, X., 2011. ACS Nano 5, 3831–3838.
Zhang, K., Lv, S., Lin, Z., Tang, D., 2017. Biosens. Bioelectron. 95, 34–40.
Zhang, L., Wang, W., Chen, Z., Zhou, L., Xu, H., Zhu, W., 2007. J. Mater. Chem. 17, 2526–2532.
Zhang, L., Wang, W., Zhou, L., Xu, H., 2010. Small 3, 1618–1625.
Zhang, T., Ma, N., Ali, A., Wei, Q., Wu, D., Ren, X., 2018. Biosens. Bioelectron. 119, 176–181.
Zhang, X., Liu, M., Mao, Y., Xu, Y., Niu, S., 2014. Biosens. Bioelectron. 59, 21–27.
Zhang, X., Zhang, L., Hu, J.S., Pan, C.L., Hou, C.M., 2015. Appl. Surf. Sci. 346, 33–40.
Zhang, Y., Zhang, N., Tang, Z.R., Xu, Y.J., 2013. Chem. Sci. 4, 1820–1824.
Zhang, Z., Wang, W., Meng, S., Yin, W., 2010. J. Hazard. Mater. 177, 1013–1018.
Zhao, W.W., Xu, J.J., Chen, H.Y., 2015. Chem. Soc. Rev. 44, 729–741.
Zhao, W.W., Xu, J.J., Chen, H.Y., 2017. Anal. Chem. 90, 615–627.
Zheng, L., Xiong, L., Li, Y., Xu, J., Kang, X., Zou, Z., Yang, S., Xia, J., 2013. Sens. Actuator B-Chem. 177, 344–349.
Zhou, Z., Hao, N., Zhang, Y., Hua, R., Qian, J., Liu, Q., Li, H., Zhu, W., Wang, K., 2017. Chem. Commun. 53, 7096–7099.
Zhu, Q., Cai, F., Zhang, J., Zhao, K., Deng, A., Li, J., 2016. Biosens. Bioelectron. 86, 899–906.